ACS OMEGA

http://pubs.acs.org/journal/acsodf

Article

Graphene Oxide−Crospolyvinylpyrrolidone Hybrid Microspheres for the Efficient Adsorption of 2,4,6-Trichlorophenol

Xiaofei Lv and Sifang Li*

Cite This: *ACS Omega* 2020, 5, 18862−18871

Read Online

ACCESS | Metrics & More | Article Recommendations | Supporting Information

ABSTRACT: Microspheres of the graphene oxide and crospolyvinylpyrrolidone composite (GO−PVPP) were prepared via suspension polymerization and investigated for the adsorption of 2,4,6-trichlorophenol (2,4,6-TCP) from wastewater. The microspheres were thoroughly characterized using scanning electron microscopy, infrared spectroscopy, N_2 physisorption, elemental analysis, X-ray diffraction, and thermogravimetric analysis. The GO−PVPP microspheres comprised GO sheets on the surface and demonstrated good thermal stability, good swelling rate, and excellent adsorption capacity of 2,4,6-TCP (up to 466.77 mg/g). The adsorptions were determined as a function of pH, temperature, adsorbent loading, adsorption time, and initial content of 2,4,6-TCP in the solutions. The sorption kinetics was satisfactorily modeled using the pseudo-second-order rate equation, and the sorption equilibrium can be described using the Freundlich model. The 2,4,6-TCP adsorption by GO−PVPP was shown to be endothermic and spontaneous. The reusability of GO−PVPP was also demonstrated by the adsorption and desorption cycles.

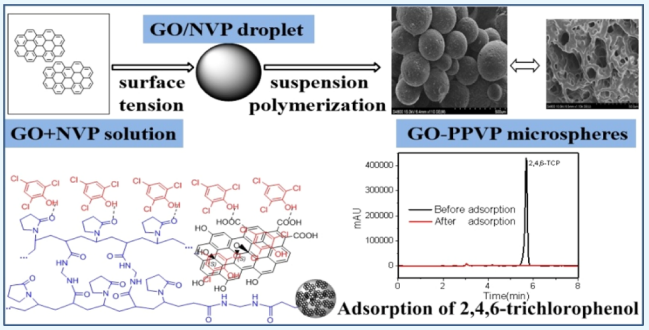

INTRODUCTION

Polyvinylpyrrolidone (PVP) has been widely used in pharmaceutical and cosmetic industries because of its biocompatibility and nontoxicity.[1−3] PVP has also been shown to exhibit excellent adsorption properties for proteins and phenol compounds for food processing.[4−7] Consequently, cross-linked PVP (crospolyvinylpyrrolidone or PVPP) can be prepared from *N*-vinylpyrrolidone (NVP) and has been explored as an adsorbent for wastewater treatment.[8] PVPP hydrogels or copolymers of NVP and other monomers have also been investigated to remove pollutants from wastewater.[9−11] Additionally, metal−organic frameworks were dispersed in PVPP to improve the adsorption efficiency for sewage treatment.[12]

Graphene oxide (GO) has attractive properties, such as high surface area, abundant surface functional groups, and good dispersibility in solvents, which provide ample possibilities to interact with metal ions, polymers, and bio-macromolecules.[13−15] For example, GO can be used to stabilize polymerization,[16,17] improve the mechanical and chemical stability of polymers,[18,19] and attain excellent shape memory properties.[20] GO has been demonstrated as an excellent adsorbent for dyes,[21,22] heavy metal ions, and other hazardous chemicals.[23−25] However, many challenges still need to be overcome to achieve full use of the adsorption properties of GO. First, it can be well dispersed in water, and thus, it cannot be easily recycled.[26] Second, its manufacturing is not environmentally friendly, and its fate in wastewater is not well understood.[27] Third, its high cost prevents a large-scale application for sewage treatment. GO composites can be an effective way to overcome these challenges. For example, the nanocomposites of GO and chitosan−poly(acrylic acid) have been reported to specifically absorb Pb(II).[28] Highly porous chitosan−gelatin monoliths strengthened by GO can also remove metal ions.[29]

2,4,6-Trichlorophenol (2,4,6-TCP) is a common contaminant as a consequence of its extensive use in pesticides, disinfectants, herbicides, and paper- and plastic-producing industries.[30,31] It is highly toxic and even carcinogenic after absorption through the skin.[32] 2,4,6-TCP can be remediated by degradation, combustion, adsorption, and others.[33,34] In particular, adsorption is attractive as it does not form secondary pollutants, unlike degradation and combustion.[35,36]

Various adsorbents have been evaluated for the adsorption of 2,4,6-TCP. For example, activated carbon has been extensively studied for 2,4,6-TCP adsorption.[37,38] However, it did not have high adsorption capacity because of the lack of favorable interactions. Many new inorganic adsorbents have been developed. For example, high carbon iron filings showed good adsorption capacity for 2,4,6-TCP and can even

Received: May 2, 2020
Accepted: July 7, 2020
Published: July 21, 2020

https://dx.doi.org/10.1021/acsomega.0c02028
ACS Omega 2020, 5, 18862−18871

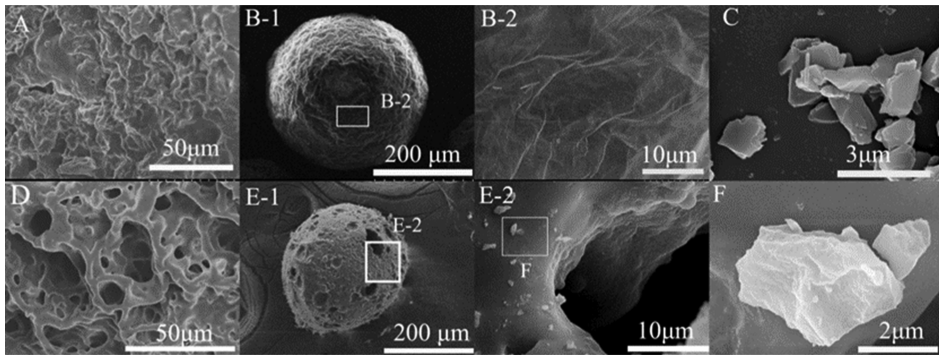

Figure 1. (A) Interior structure of PVPP microspheres. (B) Surface morphology of PVPP. (C) GO sheets in the NVP solution. (D) Interior structure of GO−PVPP microspheres. (E) Surface morphology of GO−PVPP. (F) Surface-covered GO fragment of GO−PVPP.

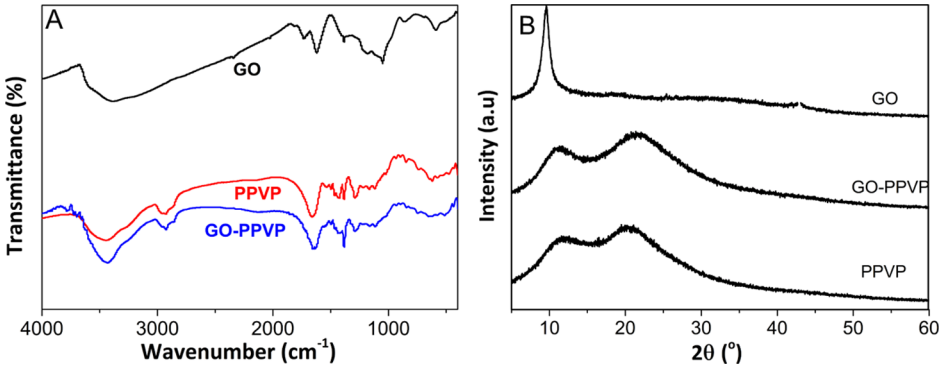

Figure 2. (A) FTIR spectra and (B) XRD patterns of GO, PVPP, and GO−PVPP.

dechlorinate 2,4,6-TCP;[39] titania−silica-mixed imidazolium-based ionic liquid and cetyltrimethyl ammonium bromide−montmorillonite have also been used to adsorb chlorophenols;[40,41] biochar prepared by sugarcane bagasse with a specific surface area of up to 361.77 m^2/g showed a 2,4,6-TCP adsorption of up to 253.38 mg/g.[42]

Low-cost polymers have provided a versatile platform as adsorbents for 2,4,6-TCP because of the flexibility in tuning the degree of hydrophilicity and porosity. For example, porous copolymers of cyanomethyl styrene−divinylbenzene prepared by suspension polymerization have been compared with the self-prepared peach stone-based activated carbon.[43] Functional polymers have been developed for 2,4,6-TCP removal, such as β-cyclodextrin-modified chitosan,[44] GO-based magnetic polymers compounded with magnetic particles and polymers, and 2,4,6-TCP-imprinted amino-functionalized nano-Fe_3O_4-polymers.[45,46] These advanced polymers comprise functional groups to chemically interact with 2,4,6-TCP. However, the adsorption capacity still needs to be further improved for practical applications.

In this study, we demonstrate that immobilizing GO in the PVPP microspheres can synergistically improve the 2,4,6-TCP adsorption capacity. The GO−PVPP microspheres were thoroughly characterized for physical properties, which were then correlated with the 2,4,6-TCP adsorption capacity and kinetics. The adsorption mechanism was elucidated, and the reusability of the adsorbents was investigated.

RESULTS AND DISCUSSION

Characterization of GO−PVPP. Figure 1 compares the scanning electron microscopy (SEM) images of PVPP and GO−PVPP microspheres. The samples were pretreated by gold spraying and were cut open to observe the cross-sectional structure. The PVPP microspheres are dense (cf. Figure 1A) and have a smooth surface (cf. Figure 1B(2)). In contrast, the GO−PVPP microspheres are porous (cf. Figure 1D,E).

The size of GO fragments in the NVP solution was generally below 5 μm (Figure 1C) because of sonication and stirring. Such small fragments can bind tightly to the polymer during NVP polymerization. Figure 1E(2),F also confirms that the GO sheets are scattered on the surface of GO−PVPP microspheres.

Figure 2A illustrates the Fourier transform infrared (FTIR) spectra of GO, PVPP, and GO−PVPP. Both PVPP and GO−PVPP show almost the same spectra, including a C−H vibration peak at 2928 cm^{-1}, a C═O vibration peak at approximately 1633 cm^{-1}, and a C−N vibration peak at 1283 cm^{-1}.[47] More importantly, GO−PVPP did not exhibit characteristic peaks of GO, such as the C−O group at 1043 cm^{-1}, −OH stretching at 1394 cm^{-1}, and C═C and C═O bonds at 1614 and 1732 cm^{-1}, respectively, presumably because of the physical interaction between the GO sheets and the polymer. Similarly, GO−PVPP and PVPP also had similar X-ray diffraction (XRD) patterns with the diffraction peaks at 11.5 and 22.5° (cf. Figure 2B).[48] The GO characteristic peak of 10° was absent for GO−PVPP, indicating the amorphous nature of the GO−PPVP adsorbent. Based on the Debye Scherer formula, the amorphous crystal grain sizes of PPVP and GO−PPVP are 11 and 17 nm, respectively, suggesting the increased grain size with GO addition.

Figure S1 displays the nitrogen adsorption and desorption curves of GO−PVPP and PVPP microspheres. The adsorption isotherms of GO−PVPP and PVPP belong to the IV type. The Brunauer−Emmett−Teller (BET) surface area for GO−PVPP

https://dx.doi.org/10.1021/acsomega.0c02028
ACS Omega 2020, 5, 18862−18871

microspheres is 10.46 m^2/g, which is almost 10 times that of PVPP (Table S1). The presence of GO in the polymer greatly increases the surface area of the microspheres, which is beneficial for adsorption. The average pore size of GO−PVPP is 28.58 nm, smaller than that of PVPP (36.71 nm). On the other hand, the pore volume of GO−PVPP (0.0092 cm^3/g) is about 3.5 times that of PVPP.

Table S2 summarizes the elemental analysis data. The contents of C and N elements in GO−PVPP are 45 and 9.66%, respectively, resulting in C/N = 4.63, which is higher than that of PVPP (3.48). The increase in the C/N ratio can be ascribed to the addition of GO (with a higher C/N ratio than PVPP) and the reduced content of the cross-linking agent (with a lower C/N ratio than the NVP monomer) during polymerization. GO can stabilize the microspheres and improve polymerization, and thus, GO−PVPP contains less cross-linking agent than PVPP.

Table S1 also records the swelling rate of water in PVPP and GO−PVPP, which is calculated based on the weight change of the microspheres after exposure to water. GO−PVPP shows a swelling rate of 272.81%, much higher than PVPP (60.40%), suggesting the looser gel networks and easier contact with the contaminants in water for GO−PVPP than PVPP.

Figure 3 compares the thermogravimetric curves for the GO−PVPP and PVPP microspheres. PVPP began to lose

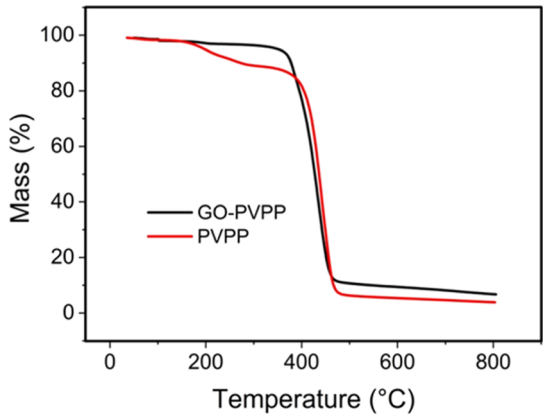

Figure 3. TGA curves of GO−PVPP and PVPP.

weight at 162 °C, and the weight loss is approximately 92% in the range of 162−450 °C, which corresponds to the thermal decomposition of PVPP. In contrast, GO−PVPP started to lose weight at 397 °C, and the weight loss is approximately 83% in the range of 397−450 °C. These results confirm that the addition of GO can significantly improve the thermal stability of the polymer (PVPP).

Effect of pH on 2,4,6-TCP Adsorption. Figure 4 illustrates the influence of pH on the equilibrium adsorption capacity of 2,4,6-TCP. As the pH increased from 2 to 10, the equilibrium adsorption capacity increased and reached its maximum at pH 4 before decreasing, which can be interpreted based on the adsorption mechanism and the actual state of 2,4,6-TCP. The pK_a value of 2,4,6-TCP is 6.23. When pH < pK_a, 2,4,6-TCP tends to exist in molecular forms in the solution and interacts with GO−PVPP by hydrogen bonds.[41] At pH > pK_a, 2,4,6-TCP became charged (Figure 4) and failed to establish hydrogen bonds with GO−PVPP,[44] decreasing the equilibrium adsorption capacity under alkaline conditions. As the pH is decreased from 6.23 to 4, the amount of 2,4,6-TCP

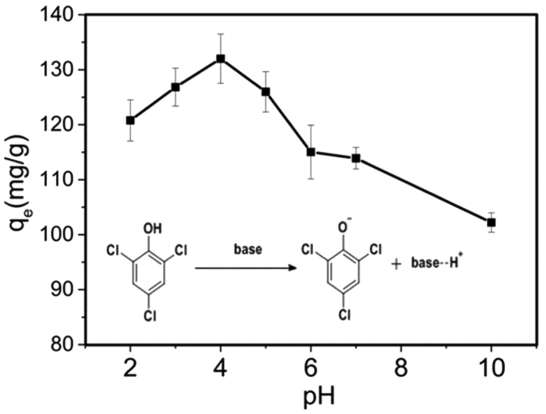

Figure 4. Effect of pH on the equilibrium adsorption capacity of 2,4,6-TCP by GO−PVPP (C_0 = 100 mg/L, T = 298.15 K, and t = 12 h).

in the molecular form increased, enhancing the adsorption capacity. However, as the pH decreased below 4, the polymer gel structures are unstable and partially destroyed, decreasing the adsorption capacity of 2,4,6-TCP.

Figure 5 shows possible mechanisms for 2,4,6-TCP adsorption by GO−PVPP. The surface is covered by the GO

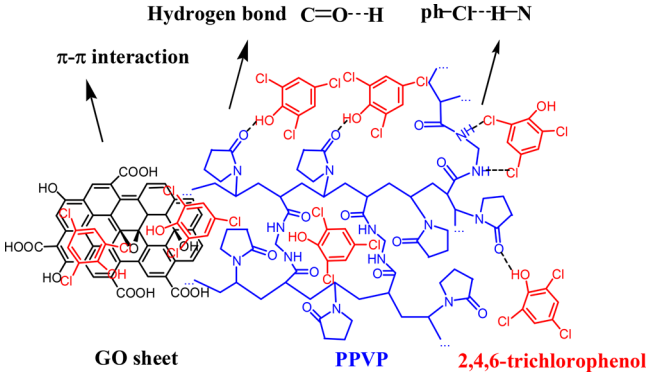

Figure 5. Possible adsorption mechanism of GO−PVPP for 2,4,6-TCP.

sheets with benzene rings, hydroxyl groups, and carboxyl groups, which provide $\pi-\pi$ interactions and hydrogen bonds with 2,4,6-TCP, leading to a much better adsorption capacity than PVPP.[49] Moreover, GO−PVPP has a much higher surface area and water absorption capacity than PVPP (cf. Table S1), which also improves the adsorption efficiency of 2,4,6-TCP.

Figure 6 compares the FTIR spectra of GO−PVPP before and after the 2,4,6-TCP adsorption. After adsorption, the peak intensity of GO−PVPP at 3441 cm^{-1} increases, which is characteristic of the stretch vibration of hydroxyl groups. The increase can be ascribed to the intermolecular hydrogen bonds formed between GO−PVPP and 2,4,6-TCP. In addition, GO−PVPP adsorbed with 2,4,6-TCP has a distinct characteristic peak at 1377 cm^{-1}, which can be interpreted as the flexural vibration of the phenolic hydroxyl group, confirming the formation of the hydrogen bonds between 2,4,6-TCP and GO−PVPP and that adsorption is effective and stable.

Influence of GO−PVPP Content. Figure 7 presents the influence of the adsorbent content on 2,4,6-TCP adsorption. When the GO−PVPP adsorbent reached 4 g/L, the removal efficiency of 2,4,6-TCP was over 99.9% and the residual

https://dx.doi.org/10.1021/acsomega.0c02028
ACS Omega 2020, 5, 18862−18871

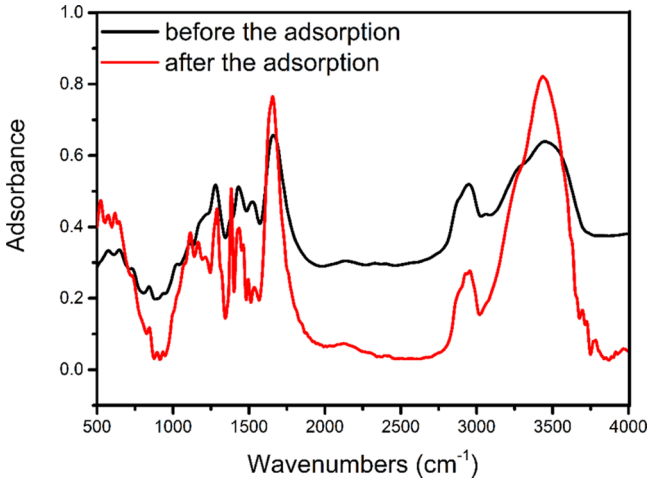

Figure 6. FTIR spectra of GO−PVPP before and after adsorption of 2,4,6-TCP.

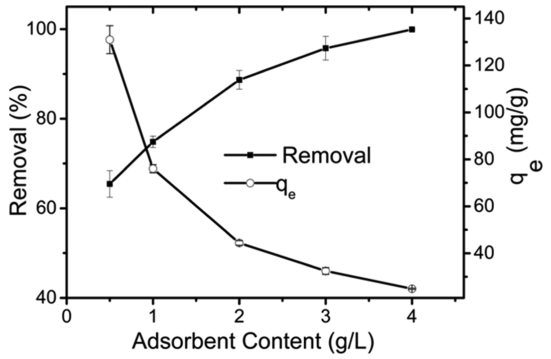

Figure 7. Effect of the adsorbent content on 2,4,6-TCP adsorption (C_0 = 100 mg/L, pH = 4, T = 298.15 K, and t = 12 h).

concentration in the solution is below the detection limit, indicating the promise of GO−PVPP for the practical treatment of 2,4,6-TCP-contaminated water. Figure 7 also displays that the q_e value of 2,4,6-TCP is reduced as the GO−PVPP content increased, which is caused by the excessive GO−PVPP adsorbent in the solution.

Kinetic Analysis for 2,4,6-TCP Adsorption. A typical expression for pseudo-first-order kinetics is shown as follows[50]

$$\frac{dq_t}{dt} = k_1(q_e - q_t) \quad (1)$$

where k_1 represents the rate constant of pseudo-first-order kinetics (min^{-1}) and q_e and q_t (mg/g) denote the mass of 2,4,6-TCP adsorbed at equilibrium and time t, respectively.

Integrating eq 1 by t from 0 to t and q_t from 0 to q_t leads to the following equation

$$\ln(q_e - q_t) = \ln q_e - k_1 t \quad (2)$$

The values of q_e and k_1 can be calculated from the intercept and slope of the linear plot of $\ln(q_e - q_t)$ against t, respectively.

The pseudo-second-order rate equation is written as follows[51]

$$\frac{dq_t}{dt} = k_2(q_e - q_t)^2 \quad (3)$$

where k_2 represents the rate constant of pseudo-second-order kinetics (g mg^{-1}·min^{-1}).

Integrating eq 3 by t from 0 to t and q_t from 0 to q_t leads to the following equation

$$\frac{t}{q_t} = \frac{1}{k_2 q_e^2} + \frac{t}{q_e} \quad (4)$$

The k_2 and q_e values can be obtained from the linear plot of t/q_t against t.

The intraparticle diffusion model is expressed as follows[52]

$$q_t = k_{ip} t^{0.5} + C \quad (5)$$

where k_{ip} represents the rate constant of intraparticle diffusion (mg g^{-1}·$min^{-1/2}$) and C is a constant (mg/g) associated with the thickness of the boundary layer. The values of k_{ip} and C can be obtained from the linear plot of q_t against $t^{0.5}$.

Figure 8A presents the results of kinetic experiments. The time required to reach equilibrium increased with increasing the initial 2,4,6-TCP concentration. For example, increasing the initial concentration from 50 to 200 mg/L increases the required time to reach equilibrium from 100 to 240 min, presumably because of more active sites on GO−PVPP to interact with 2,4,6-TCP at lower initial contents.

Figure 8B,C presents the plots of t/q_t against t and $\ln(q_e - q_t)$ against t, respectively. The related parameters and the results of the correlation analysis are listed in Table 1. The adsorption of 2,4,6-TCP on GO−PVPP microspheres appears to follow the pseudo-second-order kinetics, instead of the pseudo-first-order kinetics, because all R^2 of the former model exceeded 0.99 at different concentrations and the modeling values of equilibrium adsorption capacities were also closer to the experimental data. The good fitting with the pseudo-second-order kinetics also indicates that the adsorption of 2,4,6-TCP on GO−PVPP is mainly chemical adsorption.

The intraparticle diffusion model suggests that the plot of q_t against $t^{0.5}$ is linear and passes through the origin.[53] However, as shown in Figure 8D, the diffusion process cannot be described by only one straight line, but two or three lines (Table S3). Only two stages appear at lower initial contents of 2,4,6-TCP (50 and 100 mg/L). The first stage occurs within approximately 60 min, and the second stage occurs subsequently, presumably because the first region corresponds to the external surface adsorption and the next stage is a rate-limiting step.[54] At higher 2,4,6-TCP concentrations, there was excessive 2,4,6-TCP in the solution, which may compete for limited adsorbing sites of GO−PVPP, lowering the adsorption kinetics and reaching the final adsorption equilibrium in the third stage.[55] Nevertheless, all these different mechanisms for adsorption explain the 2,4,6-TCP sorption on GO−PVPP microspheres, including surface adsorption, chemisorption, and physical diffusion.

Adsorption Isotherms and Thermodynamics. The Langmuir model[56] and Freundlich model[57] are applied for fitting the equilibrium data of the 2,4,6-TCP adsorption by the GO−PVPP microspheres, and the equations are shown in eqs 6−8

$$\frac{C_e}{q_e} = \frac{C_e}{q_m} + \frac{1}{q_m K_L} \quad (6)$$

$$R_L = \frac{1}{K_L C_0} \quad (7)$$

https://dx.doi.org/10.1021/acsomega.0c02028
ACS Omega 2020, 5, 18862−18871

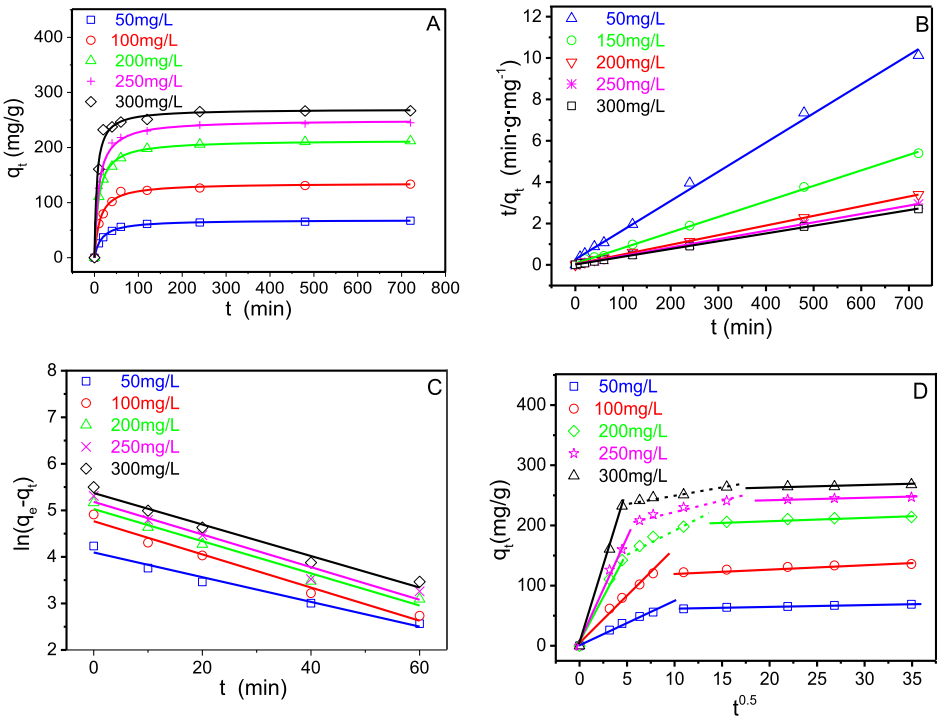

Figure 8. (A) Pseudo-second-order kinetic plots of 2,4,6-TCP on GO−PVPP at different concentrations. (B) t/q_t vs t plots of the pseudo-second-order model. (C) $\ln(q_e - q_t)$ vs t plots of the pseudo-first-order model. (D) Plots of the intraparticle diffusion model for adsorption of 2,4,6-TCP on GO−PVPP (pH = 4, GO−PVPP content = 0.5 g/L, and T = 298.15 K).

Table 1. Parameters for Pseudo-First-Order and Pseudo-Second-Order Models

		pseudo-first-order model				pseudo-second-order model			
C_0 (mg/L)	$q_{e,exp}$ (mg/g)	k_1 (min^{-1})	$q_{e,cal}$ (mg/g)	SD (mg/g)	R^2	$k_2 \times 10^3$ (g mg^{-1}·min^{-1})	$q_{e,cal}$ (mg/g)	R^2	SD (mg/g)
50	68.94	0.0265	59.73	2.142	0.9689	0.9035	68.61	0.9938	0.2234
100	135.82	0.0357	116.74	2.040	0.9740	0.5959	135.42	0.9916	0.6484
200	213.92	0.0345	151.41	3.157	0.9659	0.4681	213.56	0.9973	0.0209
250	247.77	0.0350	171.68	4.198	0.9472	0.4264	251.49	0.9959	0.1522
300	268.02	0.0358	214.86	2.1386	0.9716	0.6778	268.67	0.9929	0.1729

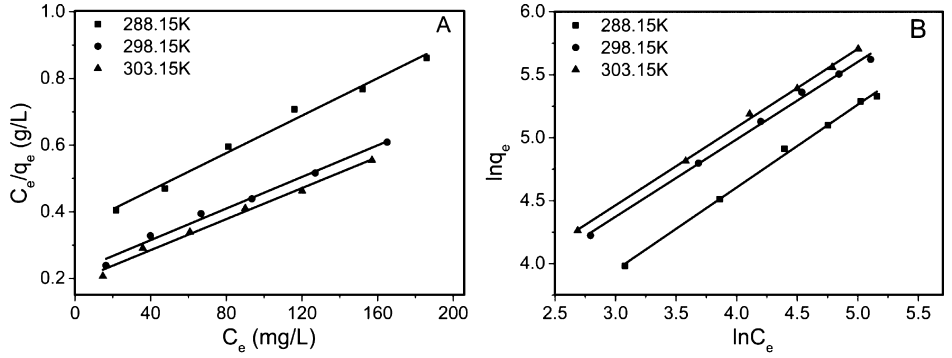

Figure 9. (A) C_e/q_e vs C_e with the data fitted using the Langmuir model. (B) ln q_e vs ln C_e with the data fitted using the Freundlich model (pH = 4, GO−PVPP content = 0.5 g/L, and t = 12 h).

$$\ln q_e = \ln K_F + \frac{1}{n} \ln C_e \tag{8}$$

where q_m (mg/g) represents the maximum adsorption capacity, K_L (L/mg) denotes the constant of the Langmuir isotherm, n is a constant related to sorption capacity and sorption intensity, and K_F (mg/g (L/mg)$^{-1/n}$) denotes the sorption affinity coefficient of the Freundlich equation.

The change in Gibbs free energy (ΔG), entropy (ΔS), and enthalpy (ΔH) can be obtained from the following equations

$$\Delta G = \Delta H - T\Delta S \tag{9}$$

$$\Delta G = -RT \ln K_D \tag{10}$$

$$K_D = \frac{C_0 - C_e}{C_e} \times \frac{V}{m} \times 1000 \tag{11}$$

https://dx.doi.org/10.1021/acsomega.0c02028
ACS Omega 2020, 5, 18862−18871

Table 2. Parameters for Langmuir and Freundlich Models

	Langmuir model					Freundlich model			
T (K)	q_{max} (mg/g)	K_L (L/mg)	R_L	R^2	SD (mg/g)	K_F (mg/g (L/mg)$^{1/n}$)	n	R^2	SD (mg/g)
288.15	413.22	0.0066	0.5051	0.9779	0.0323	7.21	1.52	0.9911	0.0206
298.15	449.88	0.0099	0.3367	0.9851	0.0347	12.53	1.63	0.9932	0.0165
303.15	466.77	0.0115	0.2898	0.9836	0.0847	13.47	1.61	0.9946	0.0144

By combining eqs 9 and 10, the following equation can be obtained

$$\ln K_D = \frac{\Delta S}{R} - \frac{\Delta H}{RT} \quad (12)$$

where T represents the temperature of the adsorbing experiment (K), K_D represents the solid−liquid partition coefficient, and R is the gas constant (8.314 J/(mol·K)).

Figure 9 displays the fitting of the adsorption isotherms with the parameters summarized in Table 2. Although the Langmuir model fits the experimental data with R^2 from 0.9779 to 0.9836, the Freundlich model offers better fitting with R^2 above 0.99 at all temperatures, suggesting that the diverse adsorption sites are distributed on the heterogeneous surface of GO−PVPP.[58] Additionally, all the values of $1/n$ are less than 1, indicating the dominance and favorability for chemisorption of 2,4,6-TCP by GO−PVPP. The formation of hydrogen bonds and $\pi-\pi$ interactions between GO−PVPP and 2,4,6-TCP are critical to the adsorption process.[45] In particular, the R_L values of the Langmuir model were calculated using eq 7 and used to determine the spontaneous state of sorption.[59] All R_L values are below 1, demonstrating that GO−PVPP microspheres are a good adsorbent for 2,4,6-TCP.

Figure 10 presents the plots of ln K_D against $1/T$ for 2,4,6-TCP sorption onto GO−PVPP microspheres, which can be used to calculate ΔH and ΔS values and thus ΔG values using eq 9 or 10. The results are summarized in Table 3. K_D is enhanced with the elevation of adsorption temperature from 288.15 to 303.15 K. The positive ΔH values indicate that the adsorption process is endothermic, while the positive ΔS values suggest the increased degree of freedom during adsorption.[42] The negative ΔG value at each temperature suggests that the adsorption process is spontaneous. Moreover, ΔG becomes more negative with increasing temperature, which reveals that the adsorption of 2,4,6-TCP becomes more favorable at higher temperatures. This result has also been confirmed by the adsorption isotherms in Figure 9 and Table 2.

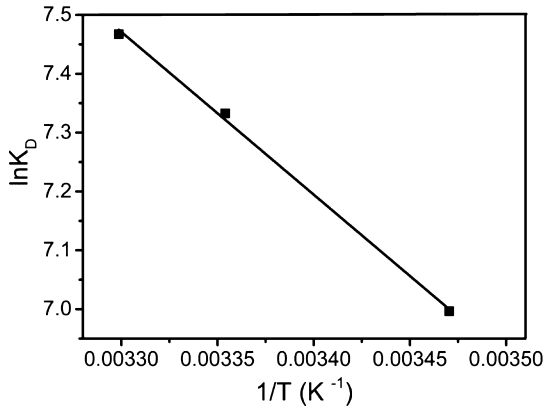

Figure 10. Effect of temperature on equilibrium adsorption coefficients.

Table 3. Thermodynamic Parameters for 2,4,6-TCP Adsorption Onto GO−PVPP

T (K)	ΔG (kJ/mol)	ΔH (kJ/mol)	ΔS (J/(mol·K)	K_D
288.15	−16.76			1092.69
298.15	−18.18	22.98	137.96	1529.35
303.15	−18.82			1741.15

The enthalpy change is in accordance with physisorption as the normal range of enthalpy change for physisorption is between 20 and 40 kJ/mol. However, in the kinetic study, the adsorption process of 2,4,6-TCP complied with pseudo-second-order kinetics, and the activation energy is very large. Therefore, adsorption is a physicochemical adsorption process rather than purely chemisorption.

Comparison of GO−PVPP with Other Adsorbents for the Adsorption of 2,4,6-TCP. Figure S2 compares the adsorption performances of GO−PVPP, PVPP, and GO with a 50 mg/L 2,4,6-TCP solution. After adsorption for 12 h, GO−PVPP, PVPP, and GO reduced the 2,4,6-TCP concentration to 0.077, 1.79, and 0.42 mg/L, respectively. GO−PVPP is the most effective adsorbent among these three materials.

Table 4 compares the maximum sorption capacity (q_m) for different adsorbents, which were calculated by the Langmuir model for accuracy. q_m for GO−PVPP reaches 466.7 mg/g, much higher than that of the other adsorbents. Such a high uptake ability of 2,4,6-TCP suggests the synergistic effect of the PVPP with a partially cross-linked structure and GO, indicating their potential for the removal of phenolic compounds from wastewater.

Table 4. Comparison of GO−PVPP with Other Materials for the Adsorption Capacity of 2,4,6-TCP

adsorbents	pH	q_{max} (mg/g)	refs
cetyltrimethyl ammonium bromide−montmorillonite	5.0	306.70	41
biochar prepared from sugarcane bagasse	2.0	253.28	42
raw lignite	3.58	56.4	43
β-cyclodextrin-6−chitosan	3.0	74.29	44
GO-based magnetic polymer	5.0	232.60	45
GO−PVPP	4.0	466.7	this study

Reusability of the GO−PVPP Adsorbents. According to the morphology and adsorption mechanism, the efficient adsorption of 2,4,6-TCP by GO−PVPP depends more or less on the surface-covered GO. The diverse functional groups of the GO sheets enhance the adsorption performance of the microspheres. Therefore, by changing the concentration of GO in the NVP solutions, such as 5, 10, and 20 mg/mL, three sets of composites coded as 5GO−PVPP, 10GO−PVPP, 20GO−PVPP were prepared to test the reusability, respectively. After

https://dx.doi.org/10.1021/acsomega.0c02028
ACS Omega 2020, 5, 18862−18871

adsorption, 2,4,6-TCP in the adsorbent was eluted by a mobile-phase solution (methanol/water = 80:20), and the GO−PVPP microspheres were dried for reuse. Five cycles were repeated in this way, and the results are exhibited in Figure 11. All three composites exhibited a slight reduction in the removal efficiency after the first cycle and then stable adsorption capabilities in the next four cycles, demonstrating the excellent reusability of the GO−PVPP microspheres and validating our approach of preparing GO-based adsorbents with a polymer skeleton.

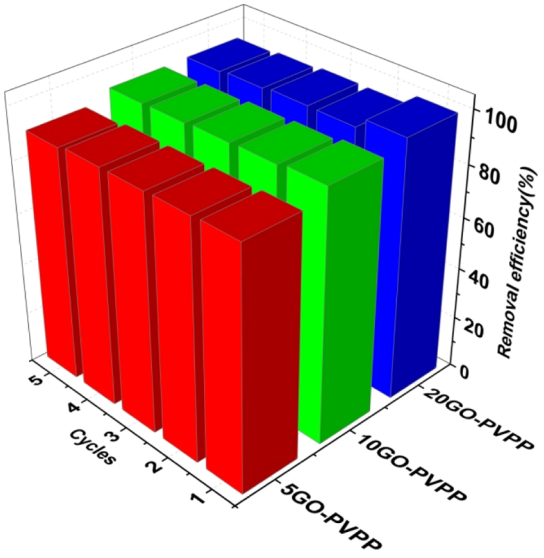

Figure 11. Removal efficiency of 2,4,6-TCP by GO−PVPP in five cycles (C_0 = 100 mg/L, T = 298.15 K, pH = 4, GO−PVPP content = 0.5 g/L, and t = 12 h).

CONCLUSIONS

In summary, the GO−PVPP microspheres were prepared by introducing GO into NVP before cross-linking polymerization. The microspheres can effectively adsorb 2,4,6-TCP in contaminated water. The adsorption performance of 2,4,6-TCP by GO−PVPP is influenced by pH, temperature, initial content of 2,4,6-TCP in the solution, and the amount of GO−PVPP. The kinetic analysis suggested that adsorption follows the pseudo-second-order rate equation, but the enthalpy change is between 20 and 40 kJ/mol, indicating a physicochemical adsorption process rather than purely chemisorption. The sorption isotherms were better described by the Freundlich model than the Langmuir model. The adsorption is endothermic and spontaneous, and the adsorption capacity increases with increasing temperature. The maximum capacity of GO−PVPP for 2,4,6-TCP sorption is 466.77 mg/g at 303.15 K and pH = 4.0. Moreover, GO−PVPP exhibited good reusability during the five cycles of adsorption and desorption, demonstrating their potential for practical applications.

EXPERIMENTAL SECTION

Materials. *N*,*N*-Methylenebisacrylamide (bisAM, 98%) and 2,4,6-TCP (98%) were obtained from Aladdin Chemical Reagent (Shanghai, China). NVP (99.9%) was purchased from Zhangzhou Huafu Chemical Industry Co. Ltd. (Fujian, China). Graphite powder, anhydrous sodium sulfate (Na_2SO_4), sulfuric acid (H_2SO_4, 98%), hydrogen peroxide (30% H_2O_2), potassium permanganate ($KMnO_4$), PVP (K30), 2,2-azobisisobutyronitrile (AIBN), and disodium hydrogen phosphate (Na_2HPO_4) were obtained from Sinopharm Chemical Reagent (Shanghai, China). Pure water (Millipore Rios-200, Billerica, MA) was used during the entire course of the experiments.

Preparation of GO−PVPP. GO was prepared using the modified Hummers method.[60] Two grams of graphite powder was added to a round bottom flask (200 mL), and 60 mL of H_2SO_4 was slowly poured into it. The temperature of the mixture was kept below 10 °C, and 9 g of $KMnO_4$ was slowly added to the flask with stirring. The mixture was then simultaneously ultrasonicated (28 kHz, 100 W) and mechanically stirred for 10 h (450 rpm, 50 °C). Subsequently, the mixture was transferred to a beaker (500 mL) and diluted five times with pure water (50 mL). Hydrogen peroxide (30%) was added until the mixture turned bright yellow, and no more bubbles were generated. The mixture was repeatedly washed and centrifuged until the pH was neutral. Finally, GO was freeze-dried for later use.

The GO−PVPP microspheres were prepared using the following procedures. First, 6 g of Na_2SO_4 was dissolved in 60 mL of water to form an aqueous solution. Second, GO (0.1 g) was added to NVP (10 mL), and the mixture was dispersed for 5 h under ultrasonic conditions (28 kHz, 100 W) at room temperature. bisAM (0.45 g) and AIBN (0.12 g) were then added to form an organic solution. Third, the Na_2SO_4 solution was added to a three-necked flask (100 mL) with a nitrogen inlet and an anchor-type stirrer (360 rpm). The NVP solution was added to the Na_2SO_4 solution in the flask at 45 °C. Nitrogen was introduced for 15 min to remove the oxygen in the system. Fourth, the temperature of the mixture in the flask was increased to 60 °C, and suspension polymerization was carried out at 60 °C for 6 h to form GO−PVPP microspheres. Finally, the microspheres were filtrated, washed with absolute ethanol and hot water (45 °C) to remove residual monomers and other impurities, and then dried under vacuum at 50 °C for 12 h.

Characterization. The morphology and structure of GO−PVPP microspheres were characterized by SEM (HITACHI S-4800), elemental analysis (Vario EL III), FT-IR (Nicolet avatar370), thermogravimetric analysis (TGA; Netzsch TG209F1), XRD (Ultima-IV), and BET analysis (TriStar II).

Adsorption Experiment and Detection. Adsorption tests were performed in a thermostatic shaker (200 rpm). GO−PVPP was added to adsorbate solutions (50 mL) with various initial concentrations of 2,4,6-TCP, including 50, 100, 200, 250, and 300 mg/L. These concentrations are lower than the solubility of 2,4,6-TCP in water (800 mg/L). The mixtures were continuously shaken for the adsorption of 2,4,6-TCP at the desired temperature. The concentration of 2,4,6-TCP in the solution was analyzed by HPLC (Agilent 1200) without preconcentration of the sample. Detailed HPLC conditions are summarized in Table S4. The standard curve of the 2,4,6-TCP solutions is linear in the concentration range of 0−250 mg/L (cf. Figure S3).

The equilibrium adsorption capacity for 2,4,6-TCP on GO−PVPP, q_e (mg/g), was determined by

$$q_e = \frac{(C_0 - C_e)V}{m} \tag{13}$$

where C_0 and C_e denote the initial and equilibrium concentrations (mg/L) of 2,4,6-TCP in solution, respectively.

https://dx.doi.org/10.1021/acsomega.0c02028
ACS Omega 2020, 5, 18862−18871

m (g) represents the weight of the GO−PVPP microspheres, and V (L) is the volume of the solution.

The removal ability of 2,4,6-TCP was based on the following formula

$$\text{removal } \% = \frac{C_0 - C_e}{C_0} \times 100\% \quad (14)$$

The determination coefficient (R^2) and standard deviation of residues (SD) were applied to evaluate the accuracy of the adsorption models[61]

$$R^2 = \left(\frac{\sum_i^n (q_{i,\text{exp}} - \overline{q}_{i,\text{exp}})^2 - \sum_i^n (q_{i,\text{exp}} - q_{i,\text{model}})^2}{\sum_i^n (q_{i,\text{exp}} - \overline{q}_{i,\text{exp}})^2} \right) \quad (15)$$

$$\text{SD} = \sqrt{\left(\frac{1}{n-p} \right) \times \sum_i^n (q_{i,\text{exp}} - q_{i,\text{model}})^2} \quad (16)$$

where $q_{i,\text{exp}}$ and $q_{i,\text{model}}$ are the adsorption capacity measured and modeled, respectively. $\overline{q}_{i,\text{exp}}$ is the average of $q_{i,\text{exp}}$ values, n is the number of experimental data, and p is the number of parameters of the fitting model.

■ ASSOCIATED CONTENT

Supporting Information

The Supporting Information is available free of charge at https://pubs.acs.org/doi/10.1021/acsomega.0c02028.

N_2 adsorption and desorption curves of GO−PVPP and PVPP, physiochemical properties of PVPP and GO−PVPP, elemental analysis of PVPP and GO−PVPP, parameters for the intraparticle diffusion model, HPLC chromatograms of 2,4,6-TCP before and after adsorption by different adsorbents (C_0 = 50 mg/L, adsorbent dosage = 1 g/L, T = 30 °C, pH = 4, and t = 6 h), detection parameters of the HPLC method for 2,4,6-TCP, HPLC standard curve of TCP solution, and chromatographic peaks of TCP standard solutions at 290 nm (PDF)

■ AUTHOR INFORMATION

Corresponding Author

Sifang Li − *Department of Chemical and Biochemical Engineering, College of Chemistry and Chemical Engineering, Xiamen University, Xiamen 361005, China;* orcid.org/0000-0002-9767-9640; Email: sfli@xmu.edu.cn

Author

Xiaofei Lv − *Department of Chemical and Biochemical Engineering, College of Chemistry and Chemical Engineering, Xiamen University, Xiamen 361005, China*

Complete contact information is available at: https://pubs.acs.org/10.1021/acsomega.0c02028

Notes

The authors declare no competing financial interest.

■ ACKNOWLEDGMENTS

This research is supported by Shanghai Wintong Ecological Engineering Co., Ltd (no. XDHT2018600A).

■ REFERENCES

(1) Guo, H.; Yang, J.; Zhao, W.; Xu, T.; Lin, C.; Zhang, J.; Zhang, L. Direct formation of amphiphilic crosslinked networks based on PVP as a marine anti-biofouling coating. *Chem. Eng. J.* **2019**, *374*, 1353−1363.

(2) Veeren, A.; Bhaw-Luximon, A.; Jhurry, D. Polyvinylpyrrolidone-polycaprolactone block copolymer micelles as nanocarriers of anti-TB drugs. *Eur. Polym. J.* **2013**, *49*, 3034−3045.

(3) Ronnander, P.; Simon, L.; Spilgies, H.; Koch, A.; Scherr, S. Dissolving polyvinylpyrrolidone based microneedle systems for in-vitro delivery of sumatriptan succinate. *Eur. J. Pharm. Sci.* **2018**, *114*, 84−92.

(4) Ferreira, S. S.; Alves, A. J.; Filipe-Ribeiro, L.; Cosme, F.; Nunes, F. M. Holistic and sustainable approach for recycling and valorization of polyvinylpolypyrrolidone used in wine fining. *ACS Sustainable Chem. Eng.* **2018**, *6*, 14599−14606.

(5) Gil, M.; Louazil, P.; Iturmendi, N.; Moine, V.; Cheynier, V.; Saucier, C. Effect of polyvinylpolypyrrolidone treatment on roses wines during fermentation: Impact on color, polyphenols and thiol aromas. *Food Chem.* **2019**, *295*, 493−498.

(6) Cai, C.; Qiu, X.; Zeng, M.; Lin, M.; Lin, X.; Lou, H.; Zhan, X.; Pang, Y.; Huang, J.; Xie, L. Using polyvinylpyrrolidone to enhance the enzymatic hydrolysis of lignocelluloses by reducing the cellulase non-productive adsorption on lignin. *Bioresour. Technol.* **2017**, *227*, 74−81.

(7) Oliveira, B. S.; de Souza D'Anzicourt, C. M.; Soares, C. M. F.; de Souza, R. L.; Lima, Á. S. Liquid-liquid extraction of phenolic compounds in systems based on acetonitrile + water + polyvinylpyrrolidone at 298.15 K. *Sep. Purif. Technol.* **2019**, *211*, 117−123.

(8) Wu, Y.-H.; Freeman, B. D. Structure, water sorption, and transport properties of crosslinked N-vinyl-2-pyrrolidone/N, N′-methylenebisacrylamide films. *J. Membr. Sci.* **2009**, *344*, 182−189.

(9) Wang, J.; Wang, X.; Zhao, G.; Song, G.; Chen, D.; Chen, H.; Xie, J.; Hayat, T.; Alsaedi, A.; Wang, X. Polyvinylpyrrolidone and polyacrylamide intercalated fybdenum disulfide as adsorbents for enhanced removal of chromium(VI) from aqueous solutions. *Chem. Eng. J.* **2018**, *334*, 569−578.

(10) Li, X.; Zhang, Z.; Fakhri, A.; Gupta, V. K.; Agarwal, S. Adsorption and photocatalysis assisted optimization for drug removal by chitosan-glyoxal/polyvinylpyrrolidone/MoS_2 nanocomposites. *Int. J. Biol. Macromol.* **2019**, *136*, 469−475.

(11) Li, M.; Wu, L.; Zhang, C.; Chen, W.; Liu, C. Hydrophilic and antifouling modification of PVDF membranes by one-step assembly of tannic acid and polyvinylpyrrolidone. *Appl. Surf. Sci.* **2019**, *483*, 967−978.

(12) Zhao, P.; Li, R.; Wu, W.; Wang, J.; Liu, J.; Zhang, Y. In-situ growth of polyvinylpyrrolidone modified Zr-MOFs thin-film nanocomposite (TFN) for efficient dyes removal. *Composites, Part B* **2019**, *176*, 107208.

(13) Kim, J.; Cote, L. J.; Kim, F.; Yuan, W.; Shull, K. R.; Huang, J. Graphene oxide sheets at interfaces. *J. Am. Chem. Soc.* **2010**, *132*, 8180−8186.

(14) Al-Gaashani, R.; Najjar, A.; Zakaria, Y.; Mansour, S.; Atieh, M. A. XPS and structural studies of high quality graphene oxide and reduced graphene oxide prepared by different chemical oxidation methods. *Ceram. Int.* **2019**, *45*, 14439−14448.

(15) Bourgeat-Lami, E.; Faucheu, J.; Noël, A. Latex routes to graphene-based nanocomposites. *Polym. Chem.* **2015**, *6*, 5323−5357.

(16) Li, J.; Deng, J.; Li, W.; Pan, K.; Deng, J. Graphene oxide (GO) as stabilizer for preparing chirally helical polyacetylene/GO hybrid microspheres via suspension polymerization. *Macromol. Rapid Commun.* **2017**, *38*, 1700452.

(17) Song, X.; Yang, Y.; Liu, J.; Zhao, H. PS colloidal particles stabilized by graphene oxide. *Langmuir* **2011**, *27*, 1186−1191.

(18) Huang, X.-H.; Zhang, M.-M.; Dou, X.-W.; Lu, X.; Qin, Y.-J.; Zhang, P.; Shi, J.-H.; Guo, Z.-X. Strengthened graphene oxide/diazoresin multilayer composites from layer-by-layer assembly and cross-linking. *Chin. Chem. Lett.* **2015**, *26*, 1155−1157.

(19) Frindy, S.; Primo, A.; Ennajih, H.; el kacem Qaiss, A.; Bouhfid, R.; Lahcini, M.; Essassi, E. M.; Garcia, H.; El Kadib, A. Chitosan-

graphene oxide films and CO_2-dried porous aerogel microspheres: Interfacial interplay and stability. *Carbohydr. Polym.* **2017**, *167*, 297−305.
(20) Panahi-Sarmad, M.; Goodarzi, V.; Amirkiai, A.; Noroozi, M.; Abrisham, M.; Dehghan, P.; Shakeri, Y.; Karimpour-Motlagh, N.; Poudineh Hajipoor, F.; Ali Khonakdar, H.; Asefnejad, A. Programing polyurethane with systematic presence of graphene-oxide (GO) and reduced graphene-oxide (rGO) platelets for adjusting of heat-actuated shape memory properties. *Eur. Polym. J.* **2019**, *118*, 619−632.
(21) Ramesha, G. K.; Vijaya Kumara, A.; Muralidhara, H. B.; Sampath, S. Graphene and graphene oxide as effective adsorbents toward anionic and cationic dyes. *J. Colloid Interface Sci.* **2011**, *361*, 270−277.
(22) Yang, S.-T.; Chen, S.; Chang, Y.; Cao, A.; Liu, Y.; Wang, H. Removal of methylene blue from aqueous solution by graphene oxide. *J. Colloid Interface Sci.* **2011**, *359*, 24−29.
(23) Li, J.; Zhang, S.; Chen, C.; Zhao, G.; Yang, X.; Li, J.; Wang, X. Removal of Cu(II) and fulvic acid by graphene oxide nanosheets decorated with Fe_3O_4 nanoparticles. *ACS Appl. Mater. Interfaces* **2012**, *4*, 4991−5000.
(24) Liu, M.; Chen, C.; Hu, J.; Wu, X.; Wang, X. Synthesis of magnetite/graphene oxide composite and application for cobalt(ii) removal. *J. Phys. Chem. C* **2011**, *115*, 25234−25240.
(25) Bao, C.; Bi, S.; Zhang, H.; Zhao, J.; Wang, P.; Yue, C. Y.; Yang, J. Graphene oxide beads for fast clean-up of hazardous chemicals. *J. Mater. Chem. A* **2016**, *4*, 9437−9446.
(26) Shen, Y.; Fang, Q.; Chen, B. Environmental applications of three-dimensional graphene-based macrostructures: adsorption, transformation, and detection. *Environ. Sci. Technol.* **2015**, *49*, 67−84.
(27) An, W.; Zhang, Y.; Zhang, X.; Li, K.; Kang, Y.; Akhtar, S.; Sha, X.; Gao, L. Ocular toxicity of reduced graphene oxide or graphene oxide exposure in mouse eyes. *Exp. Eye Res.* **2018**, *174*, 59−69.
(28) Medina, R. P.; Nadres, E. T.; Ballesteros, F. C.; Rodrigues, D. F. Incorporation of graphene oxide into a chitosan-poly(acrylic acid) porous polymer nanocomposite for enhanced lead adsorption. *Environ. Sci.: Nano* **2016**, *3*, 638−646.
(29) Zhang, N.; Qiu, H.; Si, Y.; Wang, W.; Gao, J. Fabrication of highly porous biodegradable monoliths strengthened by graphene oxide and their adsorption of metal ions. *Carbon* **2011**, *49*, 827−837.
(30) Jarvinen, K. T.; Melin, E. S.; Puhakka, J. A. High-rate bioremediation of chlorophenol-contaminated groundwater at low temperatures. *Environ. Sci. Technol.* **1994**, *28*, 2387−2392.
(31) Benitez, F. J.; Beltran-Heredia, J.; Acero, J. L.; Rubio, F. J. Chemical decomposition of 2,4,6-trichlorophenol by ozone, Fenton's reagent, and UV radiation. *Ind. Eng. Chem. Res.* **1999**, *38*, 1341−1349.
(32) Nichkova, M.; Marco, M.-P. Biomonitoring human exposure to organohalogenated substances by measuring urinary chlorophenols using a high-throughput screening (HTS) immunochemical method. *Environ. Sci. Technol.* **2006**, *40*, 2469−2477.
(33) Chu, W.; Rao, Y. F.; Kwan, C. Y.; Choy, W. K. Photochemical degradation of 2,4,6-trichlorophenol in the Brij 35 Micellar solution: pH control on product distribution. *Ind. Eng. Chem. Res.* **2009**, *48*, 10211−10216.
(34) Kuśmierek, K.; Sprynskyy, M.; Świątkowski, A. Raw lignite as an effective low-cost adsorbent to remove phenol and chlorophenols from aqueous solutions. *Sep. Sci. Technol.* **2020**, *55*, 1741−1751.
(35) Zhang, Q.; Yu, W.; Zhang, R.; Zhou, Q.; Gao, R.; Wang, W. Quantum chemical and kinetic study on dioxin formation from 2,4,6-TCP and 2,4,6-DCP precursors. *Environ. Sci. Technol.* **2010**, *44*, 3395−3403.
(36) Xu, F.; Yu, W.; Zhou, Q.; Gao, R.; Sun, X.; Zhang, Q.; Wang, W. Mechanism and direct kinetic study of the polychlorinated dibenzo-p-dioxin and dibenzofuran formations from the radical/radical cross-condensation of 2,4-dichlorophenoxy with 2,4-chlorophenoxy and 2,4,6-trichlorophenoxy. *Environ. Sci. Technol.* **2011**, *45*, 643−650.
(37) Knappe, D. R. U.; Matsui, Y.; Snoeyink, V. L.; Roche, P.; Prados, M. J.; Bourbigot, M.-M. Predicting the capacity of powdered activated carbon for trace organic compounds in natural waters. *Environ. Sci. Technol.* **1998**, *32*, 1694−1698.
(38) Hung, H. W.; Lin, T. F. Predicting the adsorption capacity and isotherm curvature of organic compounds onto activated carbons in natural waters. *Environ. Technol.* **2006**, *27*, 255−267.
(39) Sinha, A.; Bose, P. Interaction of 2,4,6-trichlorophenol with high carbon iron filings: Reaction and sorption mechanisms. *J. Hazard. Mater.* **2009**, *164*, 301−309.
(40) Ismail, N. A.; Bakhshaei, S.; Kamboh, M. A.; Abdul Manan, N. S.; Mohamad, S.; Yilmaz, M. Adsorption of phenols from contaminated water through titania-silica mixed imidazolium based ionic liquid: Equilibrium, kinetic and thermodynamic modeling studies. *J. Macromol. Sci., Part A: Pure Appl.Chem.* **2016**, *53*, 619−628.
(41) Yang, Q.; Gao, M.; Zang, W. Comparative study of 2,4,6-trichlorophenol adsorption by montmorillonites functionalized with surfactants differing in the number of head group and alkyl chain. *Colloids Surf., A* **2017**, *520*, 805−816.
(42) Mubarik, S.; Saeed, A.; Athar, M. M.; Iqbal, M. Characterization and mechanism of the adsorptive removal of 2,4,6-trichlorophenol by biochar prepared from sugarcane baggase. *J. Ind. Eng. Chem.* **2016**, *33*, 115−121.
(43) Simsek, E. B.; Aytas, B.; Duranoglu, D.; Beker, U.; Trochimczuk, A. W. A comparative study of 2-chlorophenol, 2,4-dichlorophenol, and 2,4,6-trichlorophenol adsorption onto polymeric, commercial, and carbonaceous adsorbents. *Desalin. Water Treat.* **2016**, *57*, 9940−9956.
(44) Zhou, L.-C.; Meng, X.-G.; Li, J.-M.; Hu, W.; Liu, B.; Du, J. Kinetics and thermodynamics of adsorption of chlorophenols onto *β*-cyclodextrin modified chitosan. *Acta Phys.-Chim. Sin.* **2012**, *28*, 1615−1622.
(45) Chen, M.-L.; Min, J.-Q.; Pan, S.-D.; Jin, M.-C. Surface core-shell magnetic polymer modified graphene oxide-based material for 2,4,6-trichlorophenol removal. *RSC Adv.* **2014**, *4*, 63494−63501.
(46) Shen, H.-Y.; Chen, Z.-X.; Li, Z.-H.; Hu, M.-Q.; Dong, X.-Y.; Xia, Q.-H. Controlled synthesis of 2,4,6-trichlorophenol-imprinted amino-functionalized nano-Fe_3O_4-polymer magnetic composite for highly selective adsorption. *Colloids Surf., A* **2015**, *481*, 439−450.
(47) Abou_Taleb, M. H. Thermal and spectroscopic studies of poly(N-vinyl pyrrolidone)/poly(vinyl alcohol) blend films. *J. Appl. Polym. Sci.* **2009**, *114*, 1202−1207.
(48) Liu, H.-G.; Lee, Y.-I.; Qin, W.-P.; Jang, K.; Feng, X.-S. Studies on composites formed by europium complexes with different ligands and polyvinylpyrrolidone. *Mater. Lett.* **2004**, *58*, 1677−1682.
(49) Wei, D.; Zhao, C.; Khan, A.; Sun, L.; Ji, Y.; Ai, Y.; Wang, X. Sorption mechanism and dynamic behavior of graphene oxide as an effective adsorbent for the removal of chlorophenol based environmental-hormones: A DFT and MD simulation study. *Chem. Eng. J.* **2019**, *375*, 121964.
(50) Ho, Y. S.; McKay, G. A comparison of chemisorption kinetic models applied to pollutant removal on various sorbents. *Process Saf. Environ. Prot.* **1998**, *76*, 332−340.
(51) Ho, Y. S.; McKay, G. Pseudo-second order model for sorption process. *Process Biochem.* **1999**, *34*, 451−465.
(52) Weber, W. J.; Morris, J. C. Kinetics of adsorption on carbon from solution. *J. Sanit. Eng. Div., Am. Soc. Civ. Eng.* **1963**, *89*, 31−60.
(53) Hameed, B. H.; Tan, I. A. W.; Ahmad, A. L. Adsorption isotherm, kinetic modeling and mechanism of 2,4,6-trichlorophenol on coconut husk-based activated carbon. *Chem. Eng. J.* **2008**, *144*, 235−244.
(54) Cheung, W. H.; Szeto, Y. S.; McKay, G. Intraparticle diffusion processes during acid dye adsorption onto chitosan. *Bioresour. Technol.* **2007**, *98*, 2897−2904.
(55) Ofomaja, A. E. Intraparticle diffusion process for lead(II) biosorption onto mansonia wood sawdust. *Bioresour. Technol.* **2010**, *101*, 5868−5876.
(56) Langmuir, I. The adsorption of gases on plane surfaces of glass, mica and platinum. *J. Am. Chem. Soc.* **1918**, *40*, 1361−1403.
(57) Freundlich, H. M. F. Over the adsorption in solution. *J. Phys. Chem.* **1906**, *57*, 385−471.

https://dx.doi.org/10.1021/acsomega.0c02028
ACS Omega 2020, 5, 18862−18871

(58) Pan, S.-D.; Shen, H.-Y.; Zhou, L.-X.; Chen, X.-H.; Zhao, Y.-G.; Cai, M.-Q.; Jin, M.-C. Controlled synthesis of pentachlorophenol-imprinted polymers on the surface of magnetic graphene oxide for highly selective adsorption. *J. Mater. Chem. A* **2014**, *2*, 15345−15356.
(59) Xu, M.; Yin, P.; Liu, X.; Dong, X.; Xu, Q.; Qu, R. Preparation, characterization, adsorption equilibrium, and kinetics for Gold-Ion adsorption of spent buckwheat hulls modified by organodiphosphonic acid. *Ind. Eng. Chem. Res.* **2013**, *52*, 8114−8124.
(60) Hummers, W. S.; Offeman, R. E. Preparation of graphite oxide. *J. Am. Chem. Soc.* **1958**, *80*, 1399.
(61) Lima, É.; Adebayo, M. A.; Machado, F. M. Kinetic and Equilibrium Models of Adsorption. In *Carbon Nanomaterials as Adsorbents for Environmental and Biological Applications*; Bergmann, C. P., Machado, F. M., Eds.; Springer: Switzerland, 2015; pp 33−69.

https://dx.doi.org/10.1021/acsomega.0c02028
ACS Omega 2020, 5, 18862−18871